



Mitigation of stimulated Raman amplification artifact in transient absorption spectroscopy

Nirankush Roy¹ · Ayon Jyoti Karmakar¹ · Prasanta Kumar Datta¹

Received: 10 April 2024 / Accepted: 15 July 2024 / Published online: 26 July 2024
© The Author(s), under exclusive licence to Springer-Verlag GmbH Germany, part of Springer Nature 2024

Abstract

Artifacts due to nonlinear optical processes like "Cross Phase Modulation (XPM)", "Stimulated Raman Amplification (SRA)", and "Two-Photon Absorption (TPA)" etc., have a detrimental effect on Transient Absorption Spectroscopy (TAS). In this study, we investigate the transient response of distilled water to explore the nature of SRA artifacts. The supercontinuum probe, generated in a sapphire crystal pumped by 808 nm, 50 fs laser pulse, is approximated as a linearly chirped Gaussian with a chirp parameter of 36. The chirp in the probe affects the TAS data, because the different spectral components of the probe arrive at different times, even at zero delay. The process of eliminating the effect of this chirp on the TAS data is successfully implemented. The method presented here will be useful to correct the dynamics of several processes of light-matter interactions such as coherence phenomena, electron–electron scattering and electron–phonon scattering. We successfully eliminated the SRA artifact from the TA dynamics of silver nanoparticles dispersed in water. Also, the imaginary part of the third-order nonlinear susceptibility ($\chi_{lm}^{(3)}$) of water is extracted to be $2.088 \times 10^{-23} \text{ m}^2/\text{V}^2$, using the SRA artifacts.

1 Introduction

Transient Absorption Spectroscopy (TAS) is a great tool for probing various ultrafast processes such as electron–hole [1, 2], exciton [3, 4], phonon [5], and chemical reaction [6, 7] dynamics in the femtosecond regime. This is a pump-probe technique, where the sample is excited by an intense, relatively narrow band pump pulse, and a weaker, broadband probe pulse measures the transition probabilities of the material. The absorption of the pump introduces a population in the higher energy states of the material, and the delayed weak probe tests the transition probability. A mechanical stage controls the pump-probe delay, and the probe spectrum is detected at each time step.

The signal in TAS is recorded in units of ΔOD (optical density), which is defined as the differential absorption of

the probe passing through the material in the presence and absence of the pump pulse, [8]

$$\Delta OD(\lambda, \tau) = A_{\text{with-pump}}(\lambda, \tau) - A_{\text{no-pump}}(\lambda) = \log \frac{I_{\text{no-pump}}^{\text{probe}}(\lambda)}{I_{\text{with-pump}}^{\text{probe}}} \quad (1)$$

where $A(\lambda, \tau)$ is the absorbance of the probe pulse at a delay τ between the pump and probe. The absorbance is defined in terms of the reflectance (R) and transmittance (T) as:-

$$A = -\log(R + T) \quad (2)$$

For our current study, the reflectance is negligible, and transmittance is given by $\frac{I_t}{I_0}$. Therefore, the absorbance in terms of input (I_0) and transmitted (I_t) intensity is:-

$$A = -\log \frac{I_t}{I_0} \quad (3)$$

Different processes in the sample give rise to different types of transient absorption signals. Depending on the sign of ΔOD signal, it can be determined whether the probe experiences either increased or decreased absorption inside the material in the presence of the pump. For example, if a certain spectral component of the probe experiences more absorption in the presence of the pump, it will result in a positive ΔOD and vice-versa.

✉ Prasanta Kumar Datta
pkdatta@phy.iitkgp.ac.in

Nirankush Roy
nirankushjnv@gmail.com

Ayon Jyoti Karmakar
ayonjyotikarmakar95@gmail.com

¹ Department of Physics, Indian Institute of Technology, Kharagpur 721302, West Bengal, India

In TAS, it is desirable that the substrate or solvent produce no transient absorption signal and the obtained data will solely characterize the sample of interest. Therefore, the substrate should ideally be transparent to the pump wavelength. However, in practice, even if such a substrate is chosen, there are still some unwanted signals when the pump and probe pulses temporally overlap inside the material. The pump pulse width used for excitation of the sample is typically approximately 100 fs. This results in a very high peak power of around 10 GW/cm² on the sample. The pump spot size is typically around a millimetre, which makes the peak intensity very high. Laser pulses of such high intensity easily induce nonlinear optical phenomena inside the material. Being instantaneous in nature, electronic nonlinear optical phenomena manifest as generally unwanted signals at the time of overlap of the pulses inside the material. These short-lived unwanted signals are called coherent artifacts. [9]

The major sources of coherent artifacts are nonlinear processes such as “Cross Phase Modulation (XPM)”, “Two-Photon Absorption (TPA)”, “Stimulated Raman Amplification (SRA)”, etc. [10–12] In each of these processes, the probe pulse spectrum gets modified due to the presence of the intense pump. Moreover, if the probing white light continuum contains a frequency chirp, the transient absorption measurement will have a signature of that. The chirp in the probe will cause an incorrect estimation of the temporal scale involved in the process being studied. Therefore, it is crucial to adjust the raw TA signal to eliminate the time offset introduced by the chirp.

In Sect. 2, we provide a brief theoretical description of Cross Phase Modulation and Stimulated Raman Amplification. Most of the past works on artifacts focus on Cross Phase Modulation [10, 12, 13], as it is observed in almost all systems. This manuscript, mainly focuses on the Stimulated Raman Amplification artifacts. Our experimental setup is described in detail in Sect. 3, and our results and discussions are presented in Sect. 4. The appearance of Stimulated Raman Amplification artifacts depends on factors such as the probe spectrum and the material being studied. For the current setup, distilled water, a readily available solvent that produces Raman artifacts is used. Additionally, water is used as a solvent for various of samples in TAS measurements, making this study valuable. We present a detailed discussion of the Raman artifacts observed in water in Sect. 4.2. Finally, we also demonstrate a process to calculate the imaginary part of the third-order susceptibility $\chi_{lm}^{(3)}$ from the Raman signal. The detailed procedure for eliminating the effect of chirping on the measurement is discussed. Inference on the effect of SRA artifacts on TAS data and its mitigation is discussed in Sect. 5.

2 Theoretical background

2.1 Cross Phase Modulation (XPM)

Cross Phase Modulation is a third-order nonlinear optical process in which a material’s refractive index modulates due to an intense pump pulse. When the probe overlaps with the pump inside the medium, the probe sees this modulated refractive index, which in turn causes modulation in its phase. The time derivative of the phase gives the instantaneous frequency of a pulse. Therefore, a modulation in the phase results in some alteration of the spectrum of the pulse. In XPM there is no net transfer of energy between the pump and the probe pulse. The intensity of different spectral components of the probe gets shuffled in presence of the pump. Therefore, the amplification of a certain frequency of the probe will result in the depletion of some other frequency. Since the probe pulse is very weak, the effect of Self Phase Modulation is neglected. Let us assume transform-limited Gaussian pump and probe pulse envelopes. [14]

$$\begin{aligned} A_{pump}(z, t) &= a(z, t)e^{i\phi(z,t)} \\ A_{probe}(z, t) &= b(z, t)e^{i\theta(z,t)} \end{aligned} \tag{4}$$

where,

$$\begin{aligned} a(0, t) &= a_0 e^{-\left(\frac{t-t_0}{\tau_{pump}}\right)^2} \\ b(0, t) &= b_0 e^{-\left(\frac{t}{\tau_{probe}}\right)^2} \end{aligned} \tag{5}$$

where τ is the pulse width, t_0 is the initial time delay, θ and ϕ are the corresponding phases of the envelopes assumed to be zero at $z = 0$.

The refractive index of the material gets modulated depending on the pump pulse intensity as,

$$n(z, t, \omega) = n_0(\omega) + \frac{n_2(\omega)}{2} |A_{pump}(z, t)|^2 \tag{6}$$

where $n_0(\omega)$ is the low-intensity refractive index. And the nonlinear refractive index, $n_2(\omega)$ is given by,

$$n_2(\omega) = \frac{3}{8n_0(\omega)} \chi^{(3)} \tag{7}$$

The propagation of the pulses inside the medium is governed by the following coupled differential equations [14],

$$\begin{aligned} \frac{\partial a}{\partial z} + \frac{1}{v_{pump}} \frac{\partial a}{\partial t} &= -\frac{\alpha_a a}{2} \\ \frac{\partial b}{\partial z} + \frac{1}{v_{probe}} \frac{\partial b}{\partial t} &= -\frac{\alpha_b b}{2} \end{aligned} \tag{8}$$

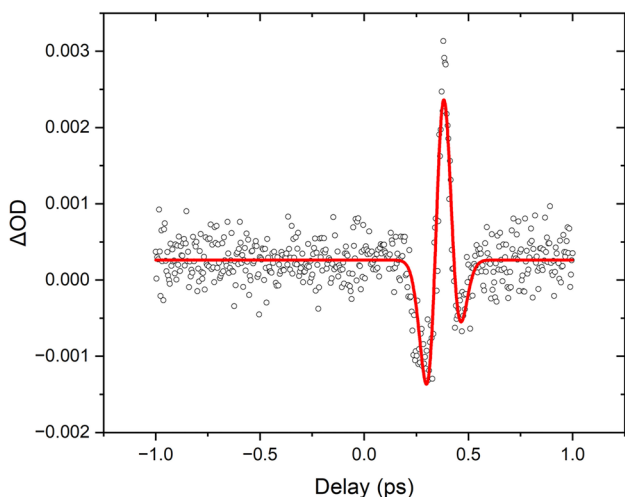


Fig. 1 Typical XPM signals in TAS for linearly chirped probe

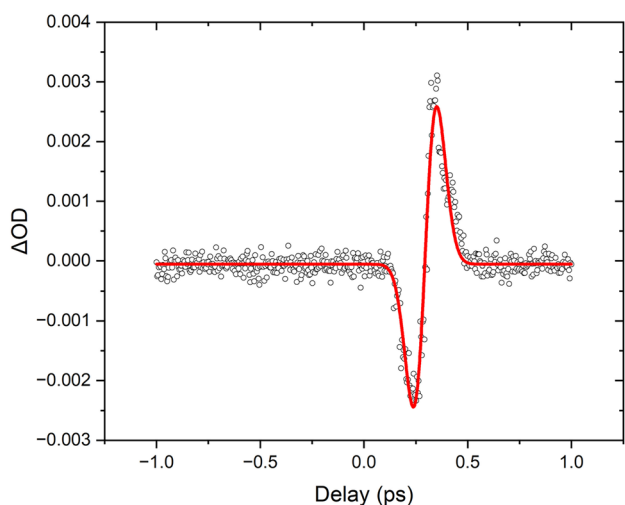


Fig. 2 Typical XPM signals in TAS for unchirped probe

$$\frac{\partial \phi}{\partial z} + \frac{1}{v_{pump}} \frac{\partial \phi}{\partial t} = \frac{n_2 \omega_{pump} \alpha^2}{c}$$

$$\frac{\partial \theta}{\partial z} + \frac{1}{v_{probe}} \frac{\partial \theta}{\partial t} = \frac{2n_2 \omega_{probe} \alpha^2}{c}$$
(9)

where α is the absorption coefficient.

By solving the above equations numerically and taking Fourier transform, the spectrum of the probe pulse can be obtained. The XPM signal observed in an empty quartz cuvette of thickness 2 mm (outside thickness, with 1 mm space in between) is shown in Figs. 1 and 2. The signal has two negative wings and a positive peak in the centre (Fig. 1) when the probe contains a chirp. The signal resembles a dispersion curve (Fig. 2) when the chirp in the probe

is negligible. More about the signal structure and its dependency on different parameters is discussed by Ekvall et al. [10]

2.2 Stimulated Raman Amplification (SRA)

Another third-order nonlinear optical phenomenon in which the scattered light has a frequency different than the input is Stimulated Raman Scattering. The difference between the frequency of the input and the scattered light is equal to the molecular vibrational frequency of the material. Scattered light with a lower frequency than of the pump is called Stokes, whereas light with a higher frequency is called anti-Stokes.

An SRA signal can be observed during TAS measurement if the probe contains certain material-specific wavelengths close to the pump wavelength. This can cause a change in the optical density for certain material-specific wavelengths. The duration of the signal is approximately the pump-probe cross-correlation time due to the instantaneous nature of the Raman Scattering process. Raman amplification is a third-order nonlinear process that couples the pump, and the probe, through interaction with the material. SRA signal is generated when the pump photon and the Stokes photon, overlap inside the medium. If the difference in energy of the two photons is equal to the molecular vibrational energy of the particular material, a stimulated emission of a third photon occurs at the Stokes frequency. In transient absorption processes, the pump photon frequency is fixed, and the Stokes photon comes from a component of the white light probe.

In Raman Scattering, the pump pulse takes the material to a virtual state. If the probe contains the Stokes frequency, the emission of a Stokes photon will be stimulated, and the Stokes frequency component of the probe will be amplified. This will result in a negative ΔOD signal. The anti-Stokes photons are generated when the molecule is already in an excited vibrational state. After going to the virtual state, it now returns to the ground state and emits a photon of higher frequency. Fig. 3 illustrates the mechanism of Stokes and anti-Stokes generation. The following equation gives the amplification of the Stokes signal in terms of the pump intensity [15],

$$A_s(z) = A_s(0)e^{\frac{gI_p z}{2}}$$
(10)

where, I_p is the pump intensity, $A_s(0)$ is the initial Stokes amplitude, z is the material thickness and g is given by,

$$g = \frac{3\omega_s}{\epsilon_0 n_s n_p c^2} \chi_{Im}^{(3)}$$
(11)

Fig. 3 **a** Stokes and **b** anti-Stokes generation in Stimulated Raman Scattering

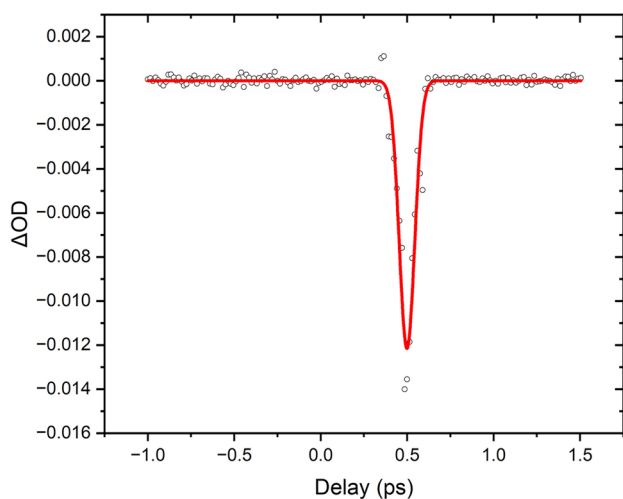
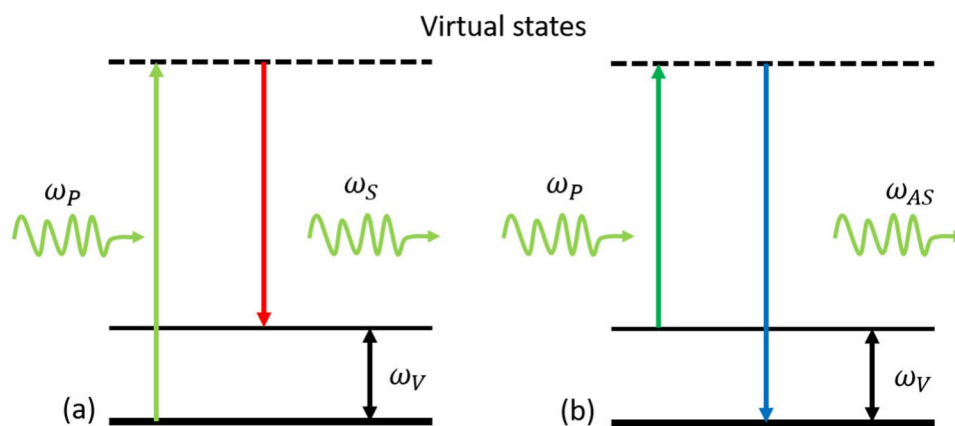


Fig. 4 Typical SRA signals in TAS at Stokes frequency

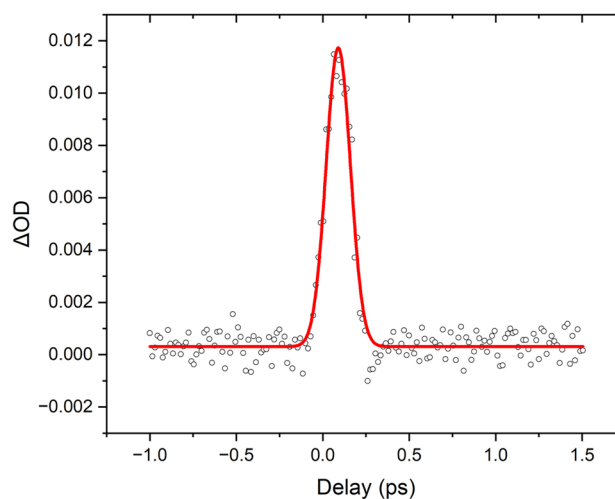


Fig. 5 Typical SRA signals in TAS at anti-Stokes frequency

where ω_s is the Stokes frequency, n_s , n_p are the refractive indices of the medium for the Stokes and Pump frequencies respectively, and $\chi_{Im}^{(3)}$ is the imaginary part of the third-order electric susceptibility. The exponential gain translates into a linear change in the TAS signal due to the logarithm in the definition of the signal. Figures 4 and 5 show the two kinds of SRA signals that can be seen in a TAS experiment. The shape of the signal is Gaussian, as expected from the cross-correlation of a Gaussian pump and probe.

3 Experiment

A 50 fs, 3 mJ Ti: Sapphire laser amplifier (Coherent Libra) having 808 nm central wavelength and 1 kHz repetition rate is used as the master laser. A tunable output from the Optical Parametric Amplifier (OPA) is used as the pump. The pump pulse width at the sample after several optical components is estimated with autocorrelation to be about 100 fs FWHM.

A sizable amount of the Libra output (70%) is coupled to the OPA. About 10% of the remaining 30% of the Libra output is focused onto a nonlinear optical crystal (Sapphire) to generate a broadband supercontinuum pulse to be used as a probe. Bandpass filters are placed before coupling the probe to the spectrometer in order to prevent the residual 808 nm pump beam from entering the spectrometer. A bandpass filter (FSR-KG5, allows 300 – 800nm to pass) is used in the current setup.

Figure 6 shows the experimental scheme used for this study. The pump laser (blue) from the OPA is passed through ND filter and aperture, then focused on the sample with a diameter of 300 microns after passing through an optical chopper. The chopper is used to modulate the beam at a frequency of 500 Hz, which is synced with the spectrometer to capture data in presence and in absence of the pump. The original beam's (red) intensity is decreased using a beam splitter, and then it passes through two retro reflectors which are mounted on a motorized stage used to control the

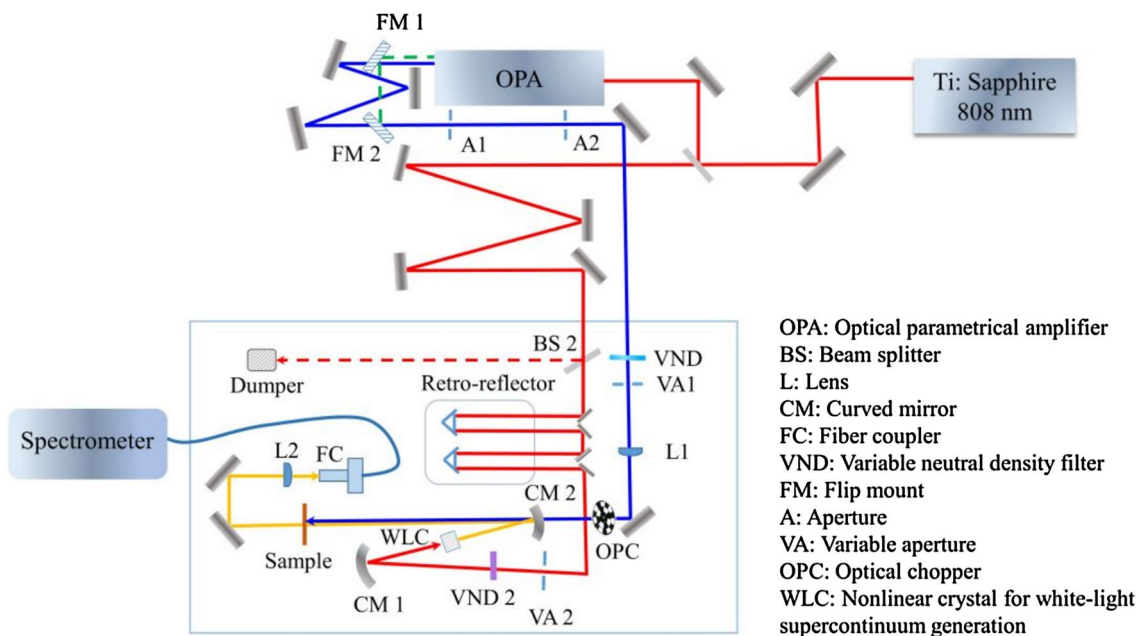


Fig. 6 Schematic diagram of the used TAS experimental set-up [8]

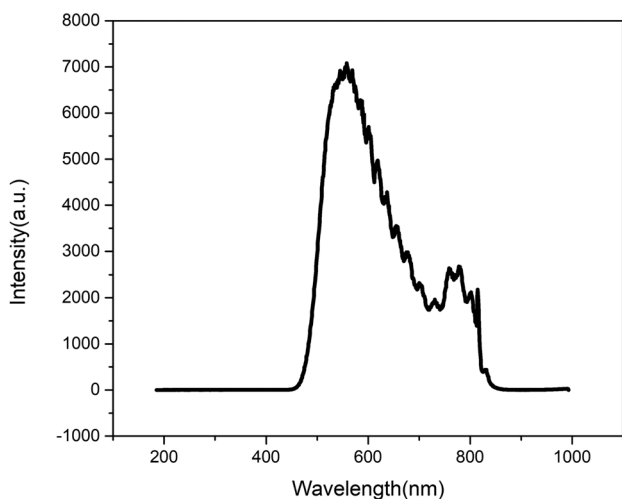


Fig. 7 Spectrum of the white light continuum generated by sapphire crystal

pump-probe delay. The beam is then focused on the sapphire crystal by a concave mirror to generate the white light supercontinuum probe (yellow). Figures 7 shows the spectrum of the generated white light supercontinuum. After that, the beam is again focused on the sample, on the region excited by the pump. The transmitted white light through the sample is collected and coupled to a spectrometer (Oriel MS 260i with Si CCD, InGaAs CCD) through a fiber coupler. The post-processing and data acquisition is performed by the Newport TAS software.

Transient absorption measurement is taken for distilled water kept inside a quartz cuvette. The total thickness of the cuvette is 2 mm, of which 1 mm is the wall made of quartz and 1 mm is the water inside the cell. Data is collected for varying pump wavelengths, keeping the average power of 1 mW, resulting in a pulse energy of 1 micro Joule. Measurements are also taken, keeping the pump wavelength fixed at 500 nm and varying the pump power.

4 Result

4.1 Chirp correction

Figures 8 and 9 show the color plot of the Transient Absorption data obtained for distilled water at 500 nm and 580 nm pump wavelengths. The data around the pump wavelength region are completely obscured due to the collection of scattered pump photons by the spectrometer and appears as a dark patch.

From a first glance at the pictures, the XPM signal is clearly visible [10]. The XPM signal is present for almost the entire probe spectrum. Figures 10 and 11 show the time traces at a particular wavelength of the probe. In the shorter wavelength part, the signal comprises of two dips (blue) and two peaks (red). This is a slightly separated version than shown in Figs. 1 and 2, because of longer distance travel in the medium of thickness 2 mm which increases the dispersion effect [10]. It is observed that the nature of the signal changes after around 600 nm. Beyond that, the

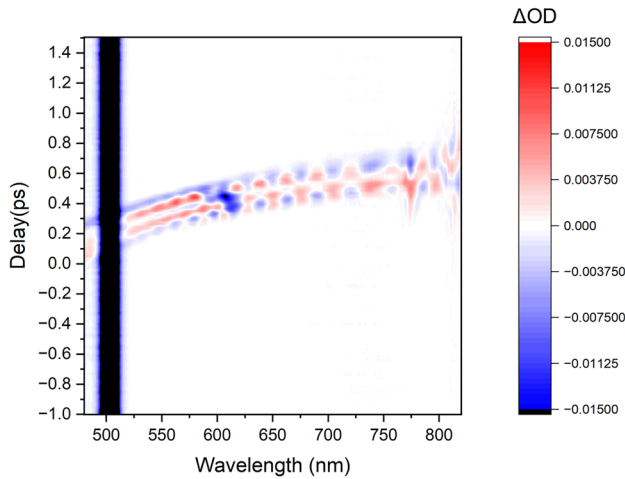


Fig. 8 SRA and XPM signals in TAS at pump wavelength 500 nm

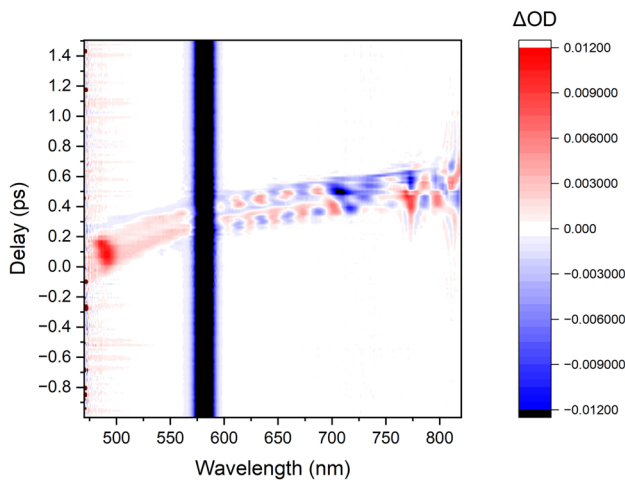


Fig. 9 SRA and XPM signals in TAS at pump wavelength 580 nm

signal becomes oscillatory, unlike the shorter wavelength case. This effect can be explained by looking at the probe spectrum in Fig. 7.

For a linearly chirped Gaussian pulse, the electric field can be represented by [16],

$$E(0, t) = \exp\left(-\frac{1 + iC}{2} \frac{t^2}{\tau^2}\right) \quad (12)$$

Here, C is the chirp parameter, and τ is the pulse width. For up-chirp, $C > 0$, and for down-chirp $C < 0$. The value of C can be estimated from,

$$\Delta\omega = \frac{(1 + C^2)^{\frac{1}{2}}}{\tau} \quad (13)$$

where $\Delta\omega$ is the spectral half-width at $1/e$ intensity point. For the probe pulse shown in Fig. 7 the value of C is about

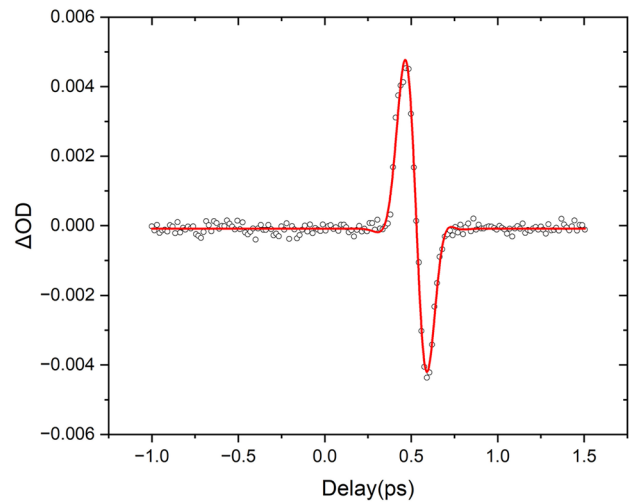


Fig. 10 Fitting of the artifacts at 675 nm probe wavelength with the Gaussian and derivatives model

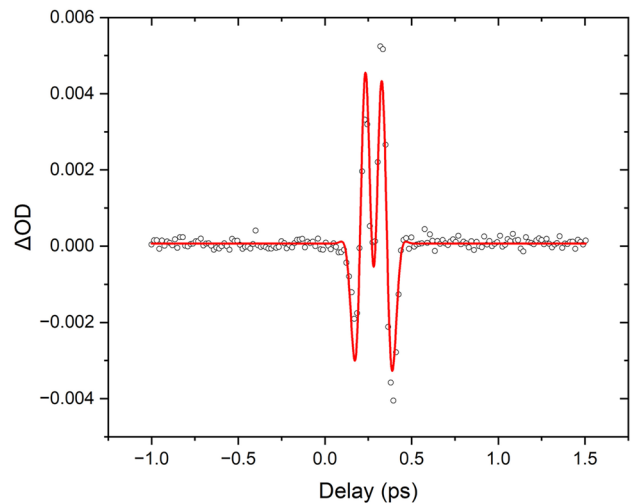


Fig. 11 Fitting of the artifacts at 530 nm probe wavelength with the Gaussian and derivatives model

36 if we consider it as a Gaussian spectrum. The spectrum is smooth up to around 600 nm, but after that it becomes bumpy. The latter part of the spectrum can be thought of as the overlapping of several narrow Gaussian spectra. For each of these narrow slices of the spectrum, the chirp parameter is very low because of the narrow bandwidth, as can be inferred from Eq. 12. Therefore, the XPM signal appears as in the case of unchirped probe, but due to the wider medium thickness, the peaks and dips are slightly separated than in Figs. 1 and 2 [10].

It should be noted that the signals in Figs. 8 and 9 appear at a relatively longer delay for longer wavelengths. Ideally, the signal for all wavelengths should appear around zero

delay. The curvature of the signal region can be attributed to the chirp in the white light continuum probe pulse. Due to the chirp, the red part of the probe pulse travels ahead of the blue part. So, the red part overlaps with the pump at a longer delay than the blue part, and the signal appears accordingly.

When studying a material, to observe the wavelength dependence of the signal at a particular delay, it is necessary to eliminate the effect of the chirp so that the signal appears around zero delay. Since the artifacts appear at the true time of overlap between the pump and a probe component, the zero-delay time for all wavelengths can be determined.

A simplified model to characterize the XPM and SRA artifacts in terms of the pump-probe cross-correlation function is the Gaussian and derivative model [11, 17],

$$\Delta OD(\omega, t) = \cos(B(t - t_0)^2 + \phi) \cdot \left[c_0 F_{cc}(\omega, t) + c_1 \frac{\partial F_{cc}(\omega, t)}{\partial t} + c_2 \frac{\partial^2 F_{cc}(\omega, t)}{\partial t^2} \right] \tag{14}$$

where $F_{cc}(\omega, t)$ is the pump-probe cross correlation function, approximated as $e^{-(t_0(\omega)-t)/\tau)^2}$ for Gaussian pump and probe pulses, t_0 is the actual zero-delay position. It is the value in the previously fixed temporal scale for the time of overlap of the pump corresponding to each probe wavelength.

The above equation is used to fit the time trace at several wavelengths over the probe spectrum. Figures 10 and 11 show examples of such fits for a pump wavelength of 500 nm. The fitting function is developed for XPM and TPA artifacts. However, since the TPA and SRA artifacts both are the shape of the cross-correlation function [12], the same function can be applied to fit SRA data also. The shown fit routine is applied for different wavelengths from the probe pulse, and the actual zero-delay position is recorded. These values of t_0 against wavelengths can be fitted with a lower degree polynomial function [18],

$$t_0(\lambda) = A + B\lambda + C\lambda^2 \tag{15}$$

Figure 12 shows the fit of the t_0 vs wavelength data with the above equation. The obtained values of the coefficients are $A = -1.5486$ ps, $B = 0.00508$ ps/nm, $C = -0.00000292$ ps/nm².

The obtained function $t_0(\lambda)$ gives the actual zero-delay position for all wavelengths in the white light supercontinuum probe pulse. Therefore, these values can be used to adjust the zero-delay position of all the wavelengths and bring them to zero (Fig. 13). This adjustment is done for the data with a 500 nm pump. Fig. 13 shows the plot of the final adjusted data after eliminating the curvature due to chirping. The initial plot (Fig. 8) is curved as the signal appears at different delays for different wavelengths. In the adjusted data, the signal is a straight line, as it starts around delay=0 for all wavelengths.

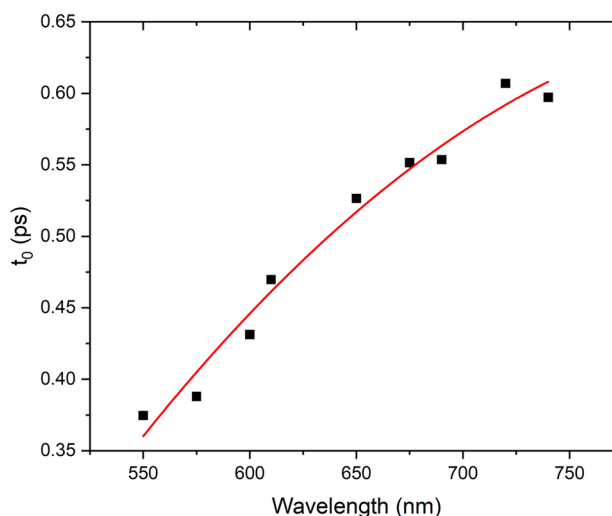


Fig. 12 t_0 vs wavelength data fitted with a polynomial function

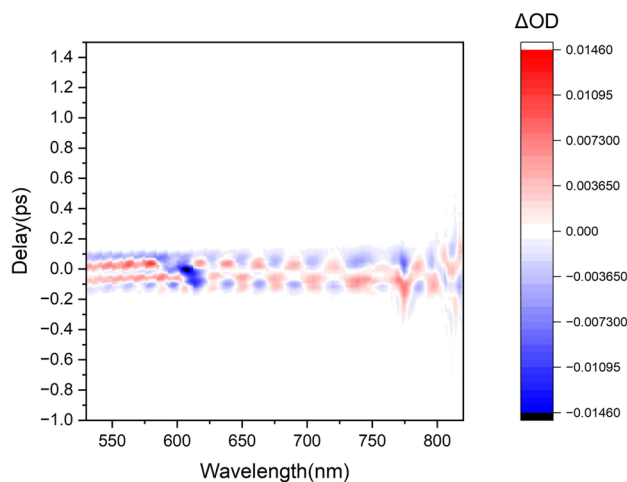


Fig. 13 Adjusted data after eliminating the effect of chirp from Fig. 8

4.2 SRA signal

In Fig. 8, there is a patch of negative signal around 607 nm. In Fig. 9 similar patches are observed around 490 nm and 715 nm. The signal for a wavelength shorter than the pump is positive, and for a wavelength longer than the pump, it is negative. Similar signals are observed for other excitation wavelengths as well. This signal can be attributed to the Stimulated Raman Amplification process occurring inside the medium.

Let us consider the particular case of pumping at 500 nm. Fig. 13 shows the chirp-adjusted color plot for this case. The spectrum at zero delay is shown in Fig. 14. The incident pump photon transfers the water molecules from the ground state to a virtual state. Upon interaction with the white light probe pulse, the emission of a Stokes photon of lower energy

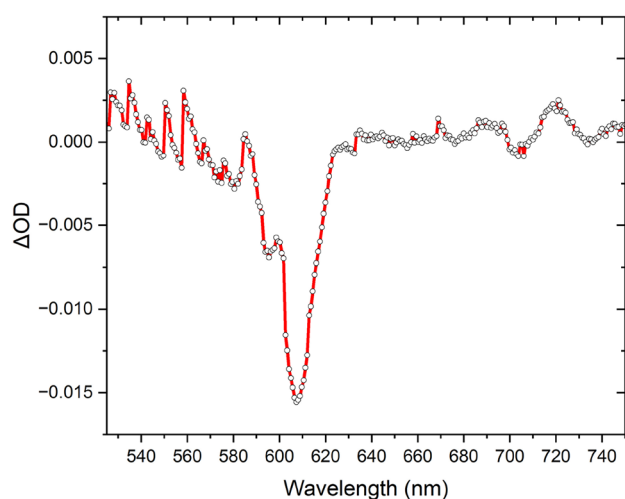


Fig. 14 Wavelength dependency of the signal at zero delay from the chirp adjusted data for 500 nm pump

than the pump (i.e., longer wavelength) is stimulated, and the molecule returns to an excited vibrational state. Thus, the energy difference between the pump photon and the emitted photon coincides with the molecular vibrational energy of water. In this manner, the light of the emission frequency in the probe pulse is amplified. An amplification of the probe translates into a negative ΔOD signal, as observed in Fig. 14.

A similar process can also cause the signal to appear at a shorter wavelength region than the pump wavelength. Contrary to the previous case, this signal is positive instead of negative as can be observed in Fig. 15. The huge dip around 645 nm is due to the scattered pump photons. The explanation for the positive signal lies in the fact that the number of water molecules in the ground state is far more than the

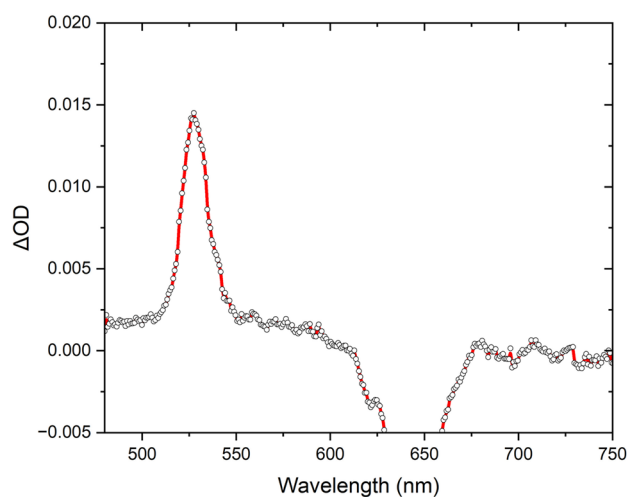


Fig. 15 Wavelength dependency of the signal at zero delay from the chirp adjusted data for 645 nm pump

number in an excited vibrational state. In Stimulated Raman Scattering, for an anti-Stokes photon to be generated, the molecule should initially be in the excited vibrational state, which, after going to the virtual state because of the pump photon, returns to the ground state, emitting a photon of higher energy. However, since the population of molecules in the excited vibrational state is low, this effect is negligible. Instead, what happens is that the component of the probe, which corresponds to the anti-Stokes frequency, now takes the molecule to a virtual state. The actual pump (pump beam used for TAS) now supplies the Stokes photon and stimulates the emission of an identical photon, leaving the molecule in an excited vibrational state. So, the probe light loses energy in this process, which appears as if light is absorbed in the material, and the transient absorption signal shows a positive peak.

It should be noted that the frequency shift due to Raman scattering is material-specific and depends on the vibrational energy of that material. Therefore, for a particular pump wavelength in TAS, the SRA signal will appear if the probe contains the Stokes or the anti-Stokes frequency for that particular case. The position of the signal shifts for different pump wavelengths, but the frequency difference between the pump and the signal remains constant. Table 1 contains the frequency shifts observed in water at various pump wavelengths.

The water molecule has three vibrational states: the O-H symmetry stretching, the O-H anti-symmetric stretching, and the H-O-H bending. As reported earlier [19], the corresponding vibrational energies are 3280 cm^{-1} , 3490 cm^{-1} , and 1654 cm^{-1} . Based on the observed values, the recorded SRA signal has contributions from both the symmetric stretching and the anti-symmetric stretching of the water molecule. In fact, these two energy states are so closely located that it is very difficult to resolve them properly.

4.3 Artifact correction

Now that the different kinds of artifacts have been identified and modelled, we can eliminate them from the raw data to

Table 1 Frequency shifts observed in distilled water at various pump wavelengths

Pump wavelength (nm)	Frequency shift for Stokes signal (cm^{-1})	Frequency shift for anti-Stokes signal (cm^{-1})
500	3499	NA
580	3255	3226
595	3384	3274
645	NA	3364
665	NA	3311

reveal the underlying dynamics. To remove the artifact, we have performed pump-probe experiment on silver nanoparticles dispersed in water pumped with 645 nm wavelength and 1 mW power.

Figure 16 shows the measured temporal trace (with artifact spike) of silver nanoparticles suspended in water for pump wavelength of 645 nm and pump power of 1 mW, at probe wavelength of 546 nm. The figure also shows the kinetics of TA of pure water at the same probe wavelength with pump power 1mW. The appearance of artifacts in this plot is shifted from the zero-delay position because of chirp. This is adjusted before artifact correction with the procedure outlined in Sect. 4.1. The data is modelled as a bi-exponential decay convoluted with the instrument response function (FWHM ~ 200 fs).

$$\Delta A = \left(A_{e-ph} e^{-\frac{t}{\tau_{e-ph}}} + A_{th} e^{-\frac{t}{\tau_{th}}} \right) * IRF \tag{16}$$

Here t_{e-ph} and t_{th} are time constants corresponding to electron-phonon scattering and thermalization respectively [20, 21]. It is difficult to fit the data with the above equation without eliminating the artifacts, and we are forced to make some approximations.

Figure 17 shows the measured artifact data and its fitting with the 'Gaussian & Derivatives' model (Eq. 14). To mitigate the artifact, we subtract the fitted function in Fig. 17 from the raw data of Fig. 16 according to the following equation. [12]

$$\Delta A_{corrected} = \Delta A_{raw} - \Delta A_r \frac{E_s}{E_r} f \tag{17}$$

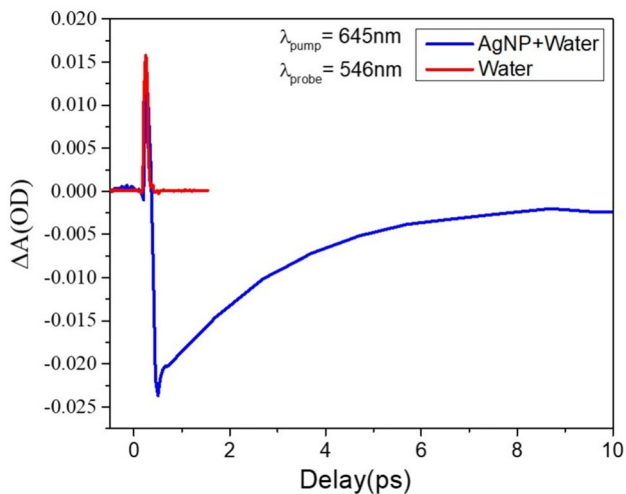


Fig. 16 TA kinetics of silver nanoparticles suspended in water for 645 nm pump wavelength and 1mW pump power at 546 nm probe wavelength(Blue). TA kinetics of pure water for 645 nm pump wavelength and 1mW pump power at 546 nm probe wavelength (red)

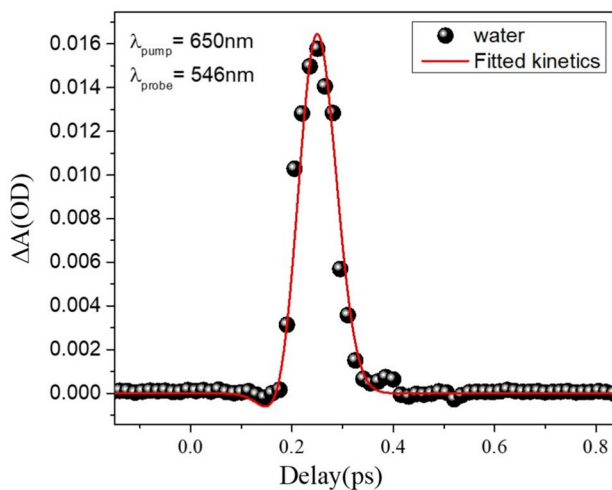


Fig. 17 SRA artifact taken at 546 nm probe wavelength pumped with 645 nm (dots). Fitting with Eq. 14 (solid line)

where, $\Delta A_{corrected}$ is the artifact free TA signal, ΔA_{raw} is the TA signal with artifact measured with pump pulse energy E_s , ΔA_r is the TA signal of pure solvent with pump pulse energy E_r . The factor f dictates the decrease of mean energy in the sample of thickness L due to stationary absorption (A) by the nanoparticles studied,

$$f = \frac{1}{L} \int_0^L 10^{-Ax} dx \tag{18}$$

Figure 18 is the TA signal before and after mitigation of the artifact, which is fitted well with Eq. 16. The obtained time constants from the fitting are $t_{e-ph} = 1.5$ ps and $t_{th} = 10.3$

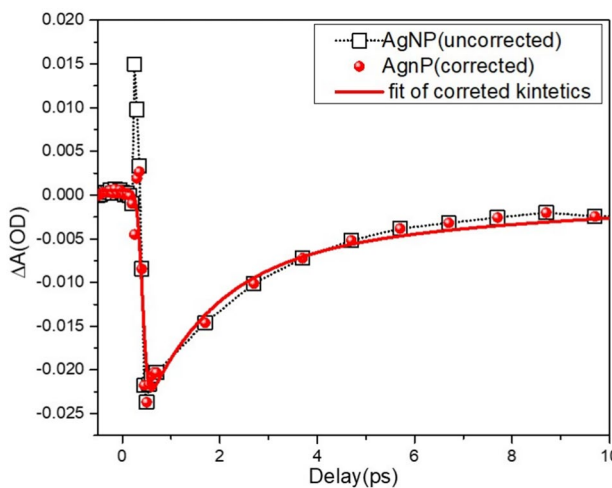


Fig. 18 TA kinetics of silver nanoparticles suspended in water at 546 nm probe wavelength before artifact correction (square and dashed line). TA kinetics after artifact correction (red circle). Fitted kinetics according to Eq. 16 (solid red line)

ps. In this particular case, the pump power used for artifact measurement and sample measurement is the same, resulting in similar intensity of both signals.

4.4 Estimation of $\chi_{Im}^{(3)}$

In stimulated Raman scattering, the signal is expected to grow according to a known function of the pump intensity. The stimulated Raman scattering is a parametric process involving the third-order nonlinearity of the material, which amplifies the Stokes field at the expense of the pump. Therefore, this pump intensity dependence of the signal can be used to estimate the nonlinearity of the solvent, i.e., water.

Since the pump intensity in the experiment is far greater than the probe, using the undepleted pump approximation as in Eq. 10, the differential absorption defined in Eq. 1 can be written as:

$$\begin{aligned} \Delta OD &= -\log \left| \frac{A_s(z)}{A_s(0)} \right|^2 = -\log \left| \frac{A_s(0)e^{\frac{gI_p z}{2}}}{A_s(0)} \right|^2 \\ &= -2 \log e^{\frac{gI_p z}{2}} \\ &= -(gz \log e)I_p \end{aligned} \tag{19}$$

For a particular pump wavelength, ω_s is constant and so g is also constant. Therefore, according to Eq. 19, ΔOD varies linearly with I_p with the slope of $-gz \log e$.

Figure 19 shows the variation of peak ΔOD value with the incident pump fluence for a pump wavelength of 500 nm. The values of ΔOD is taken positive here to represent the growth. Actually, the ΔOD is negative for the Stokes

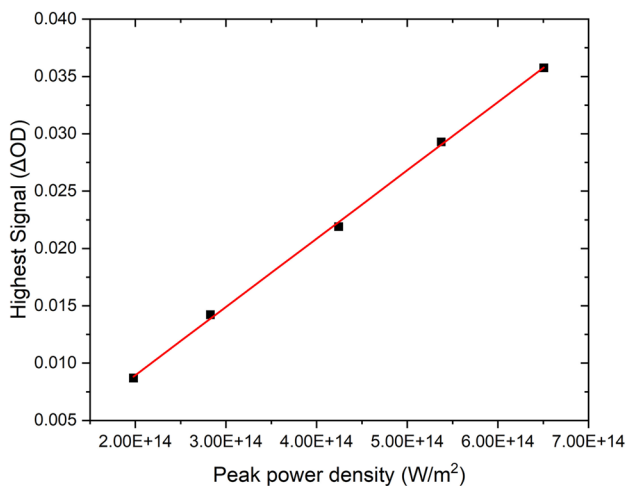


Fig. 19 Variation of the peak SRA signal with pump fluence for 500 nm pump wavelength

signal. The linear fit yields a slope of 5.96×10^{-17} . Therefore, including the negative sign for negative ΔOD values for Stokes signal, we have,

$$-5.96 \times 10^{-17} = -g \times z \times \log e \tag{20}$$

Substituting the value of $z = 1$ mm, we get,

$$5.96 \times 10^{-17} = g \times 0.001 \times \log e \tag{21}$$

This gives the value $g = 1.372 \times 10^{-13}$.

Taking $n_s = 1.3320$ and $n_p = 1.3350$ for water, and the Stokes frequency at 608 nm, the expression for g is,

$$1.372 \times 10^{-13} = \frac{3 \times 3.1 \times 10^{15}}{\epsilon_0 \times 1.332 \times 1.335 \times 9 \times 10^{16}} \chi_{Im}^{(3)} \tag{22}$$

Evaluating this, the value of $\chi_{Im}^{(3)}$ for water is obtained to be $2.088 \times 10^{-23} \text{ m}^2/\text{V}^2$. The computed result agrees very well with the value reported previously. [22]. This confirms that the presented technique can estimate the nonlinearity of the material quite reliably.

5 Conclusion

The two major sources of coherent artifacts, XPM and SRA, are studied. Experimental data is collected for solvent distilled water (H_2O) inside a 1 mm quartz cuvette. The experimental results reproduce the theoretical predictions about the artifacts. The slight discrepancy is attributed to the imperfect nature of the supercontinuum spectrum generated in sapphire crystal. The presence of the SRA signal is verified by examining the vibrational levels of water. The obtained artifacts are well-fitted with the pre-existing Gaussian and derivatives model to eliminate the effect of chirp on the data. The fitted equations can also be used to subtract the entire artifact for a particular probe wavelength when a sample is studied with the substrate to reveal the actual temporal dynamics of the system. We have successfully implemented this method to eliminate the artifacts arising in TAS measurement of silver nanoparticles suspended in water. It is also demonstrated that though unwanted in TAS experiments, the SRA artifacts can contain valuable information about the sample being studied, such as its molecular vibrational levels and third-order nonlinear susceptibility. A procedure to calculate the value of $\chi_{Im}^{(3)}$ from the SRA signal is also prescribed. Accurate modelling of the coherent artifact is vital for extracting valuable information about processes like coherent phonon dynamics, dephasing time due to electron–electron and electron–phonon scattering etc., during the initial pump-probe delay times. We believe this study will be helpful to gain further insights into this field.

Acknowledgements The authors gratefully acknowledge the UPM (SGDRI) project of IIT Kharagpur for all the equipment used in the transient absorption measurements. The authors thank Dr. Tara Singha for helpful discussions. The authors also thank Amit Kumar Pradhan and Dr. Amiya Priyam and Suman Kumar for providing Ag nanoparticles for the experiment.

Author contributions N.R. and A.K. conducted the experiment, collected data and performed the analysis and interpretation presented in this work. P.K.D. guided in the conception and design of the work. N.R. wrote the main manuscript. N.R. and P.K.D. wrote the abstract. All authors reviewed the manuscript.

Data availability The raw data for the findings reported in this manuscript is not openly available currently but may be obtained from the authors upon reasonable request.

Declarations

Conflict of interest The authors declare no competing interests.

References

1. S. Proadhan, K.K. Chauhan, T. Singha, M. Karmakar, N. Maity, R. Nadarajan, P. Kumbhakar, C.S. Tiwary, A.K. Singh, M.M. Shaijumon et al., Comprehensive excited state carrier dynamics of 2d selenium: one-photon and multi-photon absorption regimes. *Appl. Phys. Lett.* **123**(2), 123 (2023)
2. M. Karmakar, P. Kumbhakar, T. Singha, C.S. Tiwary, D. Chanda, P.K. Datta, Anomalous indirect carrier relaxation in direct band gap atomically thin gallium telluride. *Phys. Rev. B* **107**, 075429 (2023). <https://doi.org/10.1103/PhysRevB.107.075429>
3. M. Karmakar, S. Bhattacharya, S. Mukherjee, B. Ghosh, R.K. Chowdhury, A. Agarwal, S.K. Ray, D. Chanda, P.K. Datta, Observation of dynamic screening in the excited exciton states in multilayered mos_2 . *Phys. Rev. B* **103**, 075437 (2021). <https://doi.org/10.1103/PhysRevB.103.075437>
4. R.K. Chowdhury, S. Nandy, S. Bhattacharya, M. Karmakar, S.N. Bhaktha, P.K. Datta, A. Taraphder, S.K. Ray, Ultrafast time-resolved investigations of excitons and biexcitons at room temperature in layered ws_2 . *2D Materials* **6**(1), 015011 (2018)
5. K.K. Chauhan, S. Proadhan, S. Bhattacharyya, P.K. Dutta, P.K. Datta, Hot phonon and auger heating mediated slow intraband carrier relaxation in mixed halide perovskite. *IEEE J. Quantum Electron.* **57**(1), 1–8 (2020)
6. S. Bhattacharya, D.E. Nevenon, A.J. Auty, A. Graf, M. Appleby, N. Chaudhri, D. Chekulaev, C. Brückner, A.A. Chauvet, V.N. Nemykin, Photophysical exploration of two isomers of octaethyltriopyrrocorphin. *J. Phys. Chem. A* **127**(37), 7694–7706 (2023)
7. N. Tamai, H. Masuhara, Femtosecond transient absorption spectroscopy of a spirooxazine photochromic reaction. *Chem. Phys. Lett.* **191**(1–2), 189–194 (1992)
8. M. Karmakar, Ultrafast quasiparticle dynamics in layered transition metal dichalcogenides and other metal monochalcogenides. PhD thesis, IIT Kharagpur (2021)
9. M. Lebedev, O.V. Misochko, T. Dekorsy, N. Georgiev, On the nature of “coherent artifact.” *J. Expr. Theor. Phys.* **100**, 272–282 (2005)
10. K. Ekvall, P. Van Der Meulen, C. Dhollande, L.-E. Berg, S. Pommeret, R. Naskrecki, J.-C. Mialocq, Cross phase modulation artifact in liquid phase transient absorption spectroscopy. *J. Appl. Phys.* **87**(5), 2340–2352 (2000)
11. S.A. Kovalenko, A.L. Dobryakov, J. Ruthmann, N.P. Ernsting, Femtosecond spectroscopy of condensed phases with chirped supercontinuum probing. *Phys. Rev. A* **59**(3), 2369 (1999)
12. M. Lorenc, M. Ziolk, R. Naskrecki, J. Karolczak, J. Kubicki, A. Maciejewski, Artifacts in femtosecond transient absorption spectroscopy. *Appl. Phys. B* **74**, 19–27 (2002)
13. A. Bresci, M. Guizzardi, C. Valensise, F. Marangi, F. Scotognella, G. Cerullo, D. Polli, Removal of cross-phase modulation artifacts in ultrafast pump–probe dynamics by deep learning. *APL Photon.* **6**(7) (2021)
14. P. Spencer, K. Shore, Pump-probe propagation in a passive kerr nonlinear optical medium. *JOSA B* **12**(1), 67–71 (1995)
15. P.E. Powers, J.W. Haus, *Fundamentals of Nonlinear Optics* (CRC Press, New York, 2017)
16. G.P. Agrawal, Nonlinear fiber optics. In: *Nonlinear Science at the Dawn of the 21st Century*, pp. 195–211. Springer, (2000)
17. B. Baudisch, Time resolved broadband spectroscopy from uv to nir. PhD thesis, Imu (2018)
18. V.I. Klimov, D.W. McBranch, Femtosecond high-sensitivity, chirp-free transient absorption spectroscopy using kilohertz lasers. *Opt. Lett.* **23**(4), 277–279 (1998)
19. M. Stomp, J. Huisman, L. Stal, H. Matthijs, M. Stomp, J. Huisman, L.J. Stal, H.C.P. Matthijs, Colorful niches of phototrophic microorganisms shaped by vibrations of the water molecule. *The ISME J* **1**, 271–82 (2007). <https://doi.org/10.1038/ismej.2007.59>
20. S. Bhattacharya, A. Ghorai, S. Raval, M. Karmakar, A. Midya, S.K. Ray, P.K. Datta, A comprehensive dual beam approach for broadband control of ultrafast optical nonlinearity in reduced graphene oxide. *Carbon* **134**, 80–91 (2018)
21. L. Wang, S. Takeda, R. Sato, M. Sakamoto, T. Teranishi, N. Tamai, Morphology-dependent coherent acoustic phonon vibrations and phonon beat of au nanopolyhedrons. *ACS Omega* **6**(8), 5485–5489 (2021)
22. M. Thalhammer, A. Penzkofer, Measurement of third-order nonlinear susceptibilities by non-phase matched third-harmonic generation. *Appl. Phys. B* **32**, 137–143 (1983)

Springer Nature or its licensor (e.g. a society or other partner) holds exclusive rights to this article under a publishing agreement with the author(s) or other rightsholder(s); author self-archiving of the accepted manuscript version of this article is solely governed by the terms of such publishing agreement and applicable law.